Radiology: Artificial Intelligence

Automated Inline Analysis of Myocardial Perfusion MRI with Deep Learning

Journal:	*Radiology: Artificial Intelligence*
Manuscript ID	RYAI-20-0009.R2
Manuscript Type:	Technical Development
Manuscript Categorization Terms:	Adults < 1. SUBJECT MATTER, MR-Perfusion < 2. MODALITIES/TECHNIQUES, Cardiac < 4. AREAS/SYSTEMS, Heart < 5. STRUCTURES, Segmentation < 6. TOPICS, Technical Aspects < 6. TOPICS, Segmentation < Vision < Application Domain < 8. MACHINE LEARNING, Quantification < Vision < Application Domain < 8. MACHINE LEARNING, Supervised learning < Type of machine learning < 8. MACHINE LEARNING, Convolutional Neural Network (CNN) < Deep learning algorithms < Machine learning algorithms < 8. MACHINE LEARNING

Automated Inline Analysis of Myocardial Perfusion MRI with Deep Learning

Hui Xue[1], Rhodri Davies[2], Louis AE Brown[3], Kristopher D Knott[2], Tushar Kotecha[4], Marianna Fontana[4], Sven Plein[3], James C Moon[2], Peter Kellman[1]

1. National Heart, Lung and Blood Institute, National Institutes of Health, Bethesda, MD, USA
2. Barts Heart Centre, Barts Health NHS Trust, London, UK
3. Department of Biomedical Imaging Science, Leeds Institute of Cardiovascular and Metabolic Medicine, University of Leeds, Leeds, UK
4. National Amyloidosis Centre, Royal Free Hospital, London, UK

Corresponding author:

Hui Xue

National Heart, Lung and Blood Institute
National Institutes of Health
10 Center Drive, Bethesda
MD 20892
USA

Phone: +1 (301) 827-0156
Cell: +1 (609) 712-3398
Fax: +1 (301) 496-2389
Email: hui.xue@nih.gov

Word Count: 2,000

hui.xue@nih.gov
rhodri.davies2@nhs.net
kristopher.knott@nhs.net
l.brown1@leeds.ac.uk
s.plein@leeds.ac.uk
tushar.kotecha@nhs.net
m.fontana@ucl.ac.uk

This manuscript was submitted and appeared on arXiv at https://arxiv.org/abs/1911.00625 (v1, Nov 2, 2019; v2, May 29, 2020).

j.moon@ucl.ac.uk
kellmanp@nhlbi.nih.gov

Automated Inline Analysis of Myocardial Perfusion MRI with Deep Learning

Key points:

1. Proposed and validated a convolutional neural network solution for cardiac perfusion mapping and integrated an automated inline implementation on the MR scanner, enabling "one-click" analysis and reporting.

2. The large training set included 1825 perfusion series from 1034 patients (mean age 60.6 ± 14.2 years) and the independent test set included 200 scans from 105 patients (mean age 59.1 ± 12.5 years).

3. Comparison of automated and manual derived myocardial blood flow measurement showed no differences on both global and per-sector basis ($P > .80$).

Summary statement:

The described CNN was capable of segmenting and determining the mean stress and rest myocardial blood flow in a manner comparable to manual segmentation.

820 Jorie Blvd., Suite 200, Oak Brook, IL, 60523, 630-481-1071, rad-ai@rsna.org

Abbreviations

AHA = American Heart Association, CNN = convolutional neural network, CPU = central processing unit, LV = left ventricular, MBF = myocardial blood flow, RV = right ventricular

820 Jorie Blvd., Suite 200, Oak Brook, IL, 60523, 630-481-1071, rad-ai@rsna.org

Abstract

Purpose

To develop a deep neural network based computational workflow for inline myocardial perfusion analysis that automatically delineates the myocardium, which improves the clinical workflow and offers a "one-click" solution.

Methods

In this retrospective study, consecutive adenosine stress and rest perfusion scans were acquired from three hospitals between Oct 1, 2018 and Feb 27, 2019. The training and validation set included 1825 perfusion series from 1034 patients (mean age 60.6 ± 14.2 years). The independent test set included 200 scans from 105 patients (mean age 59.1 ± 12.5 years). A convolutional neural network (CNN) model was trained to segment the left ventricular cavity, myocardium, and right ventricle by processing an incoming time series of perfusion images. Model outputs were compared to manual ground-truth for accuracy of segmentation and flow measures derived on a global and per-sector basis with T-test performed for statistical significance. The trained models were integrated onto MR scanners for effective inference.

Results

The mean Dice ratio of automatic and manual segmentation was 0.93 ± 0.04. The CNN performed similarly to manual segmentation and flow measures for mean stress myocardial blood flow (MBF [ml/min/g]; 2.25 ± 0.59 vs 2.24 ± 0.59, P = .94) and mean rest MBF (1.08 ± 0.23 vs 1.07 ± 0.23, P = .83). The per-sector MBF values showed no difference between the CNN and manual assessment (P = .92). A CPU based model inference on the MR scanner took less than 1 second for a typical perfusion scan of three-slices.

Conclusions

The described CNN was capable of cardiac perfusion mapping and integrated an automated inline implementation on the MR scanner, enabling "one-click" analysis and reporting in a manner comparable to manual assessment.

820 Jorie Blvd., Suite 200, Oak Brook, IL, 60523, 630-481-1071, rad-ai@rsna.org

Introduction

Myocardial perfusion MRI has proven to be an accurate, non-invasive imaging technique to detect ischemic heart disease (1). Quantitative MR perfusion is more objective (2) and automated in-line methods (3,4) offer improved efficiency of analysis. Compared with qualitative visual assessment, quantitative methods improve the detection of disease with a global reduction in flow, as seen in balanced multi-vessel obstruction or microvascular disease (5).

Without automated segmentation of the MR perfusion maps, a reporting clinician would have to manually draw regions of interest to extract global or regional flow values. Objective perfusion assessment could be further facilitated by segmenting the myocardium to automatically generate the report leading to a "one-click" solution to improve workflow. Automated MR perfusion measurement could serve as the input for down-stream cardiovascular disease classification (6) where pre-trained CNN models receive myocardial flow and other imaging features to predict the probability of ischemic heart disease. These previous studies used manual segmentation and can be automated with the proposed approach.

In this study we propose a deep CNN based computational workflow for myocardial perfusion analysis using MRI. The right ventricular (RV) insertion points were determined to allow reporting of perfusion according to the standard 16 segment model proposed by the American Heart Association (AHA). To use the dynamic change of intensity due to contrast uptake, the proposed solution operates on the time series of two-dimensional (2D) perfusion images (referred to here as 2D+T) after respiratory motion correction. The performance of the trained CNNs was quantitatively evaluated by comparing against manually established ground-

820 Jorie Blvd., Suite 200, Oak Brook, IL, 60523, 630-481-1071, rad-ai@rsna.org

truth for both segmentation accuracy and global as well as regional flow measures on an independent hold-out test dataset.

To promote the clinical validation and adoption of the proposed solution, the trained deep learning models were integrated onto MR scanners using the Gadgetron InlineAI toolbox (7). The CNN models were applied to the acquired images as part of the scanner computing workflow (inline processing) at the time of scan, rather than as a post processing. The resulting segmentation results and analysis reports were available for immediate evaluation prior to the next image series. The method described here has been used in a prospective study of more than 1000 patients to demonstrate the prognostic significance of quantitative stress perfusion (8). A "one-click" solution to acquire free-breathing perfusion images, perform pixel-wise flow mapping, and conduct automated analysis with a 16-segment AHA report generated on the MR scanner is demonstrated.

Methods

Imaging and Data Collection

In this retrospective study, the datasets consisted of adenosine stress and rest perfusion scans which were acquired at three hospitals (_ Centre, XX; _ Hospital, XH; _ Teaching Hospitals, XHT) between Oct 1, 2018 and Feb 27, 2019. Data was acquired with the required ethical and/or audit secondary use approvals or guidelines (as per each center) that permitted retrospective analysis of anonymized data for the purpose of technical development, protocol optimization and quality control. All data was anonymized and delinked for analysis by National Institutes of Health (NIH) with approval by the NIH Office of Human Subjects Research (Exemption #13156). The collected datasets was previously included in a recent study

820 Jorie Blvd., Suite 200, Oak Brook, IL, 60523, 630-481-1071, rad-ai@rsna.org

(9) which developed a left ventricular blood pool detection solution for arterial input function images, while this study used the datasets for perfusion myocardium segmentation.

A total of 1825 perfusion scans from 1034 patients (mean age 60.6 ± 14.2 years, 692 men) were assembled and split into training and validation sets, used for CNN model training. An independent hold-out consecutive test set was assembled, consisting of 200 perfusion scans from 105 patients (mean age 59.1 ± 12.5 years, 76 men). Table 1 summarized detailed dataset information. There was no overlap between the training and validation data to the independent test data (10). Among the assembled independent test data, 96 scans were acquired at 3T scanners and 104 were from 1.5T scanners.

MRI Acquisition

Perfusion imaging used a previously published dual-sequence scheme (3). The imaging started after administering the contrast agent and acquired typical three 2D images cutting through the heart. This acquisition was repeated for every heart beat to capture the contrast passage. Details for MRI imaging can be found in Appendix E1.

Data Preparation and Ground Truth Labeling

Perfusion image series underwent motion correction and surface coil inhomogeneity correction. Resulting images were spatially upsampled to 1.0mm2 and the central field of view (176 × 176 mm2) was cropped. For the short axis perfusion slices, the LV endo- and epicardial boundaries were manually traced, together with the right ventricle (RV) (Fig. 1). Information for data preparation and labeling can be found in Appendix E2.

Model and Training

820 Jorie Blvd., Suite 200, Oak Brook, IL, 60523, 630-481-1071, rad-ai@rsna.org

The U-net semantic segmentation architecture (11,12) was adopted for the perfusion segmentation. The neural net (Fig. 2) consisted of downsampling and upsampling layers, each including a number of ResNet blocks (13) with Batch Normalization (14) and LeakyRelu (15) nonlinearity. The data for training was split into a training set (87.5% of all studies) and a validation set (12.5% of all studies). The CNN model and optimization was implemented using PyTorch (16).

The trained model was integrated to run on MR scanners using the Gadgetron Inline AI (7) streaming software. A screenshot (Fig. 3) illustrates the perfusion mapping with overlaid CNN based segmentation and AHA report, applied to a patient with reduced regional perfusion. This is a "one-click" solution for automated analysis of quantitative perfusion flow mapping.

Appendix E3 gave details about model, training and inline integration.

Statistical Analysis

The segmentation of automated processing was compared to the manually labeled test set. Performance was quantified in both segmentation accuracy and myocardial flow measures. The Dice ratio for manual label and automatic segmentation masks, was computed, together with the false positive and false negative errors. A false positive was defined as the percentage area of the segmented mask in the CNN result that was not labeled in the manual one. A false negative was defined as the percentage area of segmented mask in the manual that was not labeled in the automated result. The precision (defined as the percentage of segmented area in both the CNN and manual masks over CNN area) and recall (defined as the percentage of segmented area in both the CNN and manual masks over manual area) were also reported. The

820 Jorie Blvd., Suite 200, Oak Brook, IL, 60523, 630-481-1071, rad-ai@rsna.org

myocardium boundary errors (17), defined as the mean distance between myocardial borders of two masks, and the Hausdorff distance (18) were computed for the endo- and epicardium borders. The detection accuracy of RV insertion was measured by the angular difference between auto and manual determined direction vectors for RV insertion, as only the orientation was needed for segmentation. Global and per-sector myocardial flow measures were used quantify the CNN performance compared to manual results, displayed using Bland-Altman plots. Additionally, contours were visually inspected for segmentation failures on all 200 test scans.

Results were presented as mean ± standard deviation. T-test was performed and a *P*-value less than .05 was considered statistically significant (Matlab R2017b, Mathworks Inc., MA, USA). T-test was used to test whether there are significant differences on MBF values derived from manual and automated segmentation.

CNN Data Sharing

To encourage researchers on other platforms to adopt the proposed solution, the CNN model files, and other resources are shared openly (*https://github.com/xueh2/QPerf*).

Results

CNN Segmentation Overview and Optimization

An example of segmentation (Fig. 4) illustrates the contours overlaid on perfusion images and corresponding flow maps. The trained CNN correctly delineated the LV cavity and myocardium. The RV insertion direction was accurately detected to allow sector division. The epicardial fat, was correctly excluded from segmentation and papillary muscles were avoided.

820 Jorie Blvd., Suite 200, Oak Brook, IL, 60523, 630-481-1071, rad-ai@rsna.org

CNN and Ground Truth Segmentation Performance Comparisons

The mean Dice ratio of myocardium segmentation between CNN and manual ground-truth was 0.93 ± 0.04 (90% CI: 0.88 to 0.97). False positive and false negative rates were 0.09 ± 0.06 (90% CI: 0.02 to 0.18). and 0.06 ± 0.05 (90% CI: 0.005 to 0.13). Precision and recall were 0.92 ± 0.06 (90% CI: 0.81 to 0.97) and 0.94 ± 0.05 (90% CI: 0.87 to 0.99). The myocardium boundary error was 0.33 ± 0.15 mm (90% CI: 0.13 to 0.52 mm). Given the training image spatial resolution of 1 mm^2, the mean boundary error was less than 0.5 pixels. The mean bidirectional Hausdoff distance was 2.52 ± 1.08 mm (90% CI: 1.42 to 4.13mm) and the mean angle between auto and manually determined RV insertion point directions was 2.65 ± 3.89 degree (90% CI: 0.28 to 5.95).

The mean stress flow was 2.25 ± 0.59 ml/min/g for the CNN and 2.24 ± 0.59 ml/min/g for manual segmentation (P = .94). For rest scans, the CNN gave 1.08 ± 0.23 ml/min/g and manual measure gave 1.07 ± 0.23 ml/min/g (P = .83). The per-sector measures showed no difference between the CNN and manual measures (P = .92). Bland-Altman plots (Fig. 5) compared automatic to manual processing of MBF for both global MBF and 16-sector values.

The performance was further evaluated separately for 3 T and 1.5 T test scans. The mean Dice ratio was 0.93 ± 0.04 for 3T and 0.93 ± 0.03 for 1.5T (P = .97). At 3 T, the mean stress flow was 2.20 ± 0.59 ml/min/g for CNN and 2.21 ± 0.59 ml/min/g for manual (P = .93). The mean rest flow was 1.08 ± 0.23 ml/min/g for CNN and 1.07 ± 0.23 ml/min/g for manual (P = 0.84). At 1.5T, the mean stress flow was 2.29 ± 0.60 ml/min/g for the CNN and 2.29 ± 0.59 ml/min/g for manual (P = .97). The mean rest flow was 1.08 ± 0.23 ml/min/g for CNN and 1.07 ± 0.23 ml/min/g for manual (P = .93).

820 Jorie Blvd., Suite 200, Oak Brook, IL, 60523, 630-481-1071, rad-ai@rsna.org

Contours were visually evaluated on all 200 test scans (three slices each). There was a single stress case where one slice failed to properly segment the right ventricle, however, the myocardium was properly segmented. A second rest case had one apical slice where the myocardium segmentation included blood pool. There was apparent through-plane motion that was uncorrected. No other segmentation failures were found.

CNN Speed Performance

The CNN model was integrated on the MR scanner. On Xeon Gold, model loading time was approximately 120 ms and applying model on incomings perfusion series was approximately 250 ms per slice. For a typical three short axis acquisition, inline analysis took less than 1 second on CPU. On the older Xeon E5, model loading time was approximately 130 ms and applying models took 370 ms per slice.

Discussion

This study presents a deep neural network-based workflow for automated myocardial segmentation and reporting of the AHA 16 sector model for pixel-wise perfusion mapping. The derived myocardial measures were computed and reported inline on the MR scanner taking just one additional second of inline processing time. Quantitative evaluation in this initial study demonstrated performance of myocardial segmentation and sector-based analysis that is well matched to a human expert. This study used stress and rest data from seven scanners at three sites at 2 field strengths using over 1800 consecutive scans for training and 200 for test. Bland-Altman analysis demonstrated a 95% confidence interval for global MBF of 0.05 mmol/min/g compared to manual labeling, which is sufficient for automated detection and reporting. Prior work on segmenting perfusion (19) used much smaller datasets resulting in much higher

820 Jorie Blvd., Suite 200, Oak Brook, IL, 60523, 630-481-1071, rad-ai@rsna.org

variance. A weighted sum loss function was used in this study and gave good accuracy. There are indeed many other alternatives, such as soft Dice ratio or Focal loss (20), which can be effective in perfusion segmentation task. Which loss function is the best may vary for different applications. A comprehensive overview and implementation of many loss functions can be found at *https://github.com/JunMa11/SegLoss*.

The prognostic significance of proposed artificial intelligence application was studied and recently published in Knott et al. (8). In this study, 1049 patients with known or suspected coronary artery disease underwent stress MR perfusion scans and were analyzed with the proposed CNN models, showing reduced MBF and myocardial perfusion reserve measured automatically using artificial intelligence quantification of CMR perfusion (2). This study demonstrates the relevance of automated myocardial segmentation in CMR stress perfusion.

Automated CMR image analysis has been attempted over a long period (21). Most work focused on cine image analysis (e.g. MICCAI 2017 ACDC challenge (22), etc.) The first deep learning study which was based on a large data cohort and reported performance matching human level, was published in 2018 (23). Since then, deep neural nets were applied to other CMR imaging applications, such as T1 mapping and cardiac late enhancement segmentation (24) . Our approach utilized the temporal information through the whole bolus passage (2D+T) to exploit the contrast dynamics for detecting both RV and LV which enabled finding the RV insertion point. The epicardial fat, showing no dynamic intensity changes, was correctly excluded from segmentation which would be more difficult to avoid on a single static image.

Limitations

First, the presented study was conducted on MR scanners from a single vendor. Although the specific imaging dual-sequence used may not be available on other platforms, the

proposed segmentation method and CNN models may be still applicable. Second, although the proposed algorithm works well for the vast majority of cases, a few cases are challenging. For example, in the case of severe hypertrophy some slices may not exhibit any blood pool (ie complete extinction) where no endocardial contours are drawn. Third, the CNN models are currently trained for short-axis slices and cannot be applied to long-axis views. New training and test datasets are needed to extend segmentation to long-axis slices. In the case where the basal slice may cover some portion of out-flow tract. In this instance, the proposed algorithm will avoid the blood pool and divide a segment accordingly or may skip a segment entirely. This will result in incomplete segmentation. Fourth, in cases of severe respiratory motion that is beyond the capacity of the in-plane retrospective methods, portions of the myocardium may be blurred, where CNN segmentation can perform poorly. However, in these cases manual segmentation is difficult as well.

Another limitation of this study is the single operator for data labeling. The inter-operator reliability was not tested in this paper. Since this solution had been deployed to MR scanners, clinical collaborators have started to use this solution (8,25), but more clinical validation is required to further validate this solution.

Conclusion

In this study, we demonstrated automated analysis can be achieved on clinical scanners for perfusion MRI. Deep learning enabled inline analysis immediately after data acquisition as part of imaging computation, therefore more objective, convenient, and faster, reducing clinical burden.

820 Jorie Blvd., Suite 200, Oak Brook, IL, 60523, 630-481-1071, rad-ai@rsna.org

Appendix E1: MRI Acquisition

Perfusion imaging used a previously published dual-sequence scheme (3). A low-resolution arterial input function imaging module was inserted before the perfusion imaging and performed after the R-wave with short delay time. Typical parameters for myocardial imaging: FOV 360×270mm^2, slice thickness 8 mm, imaging matrix 192×111, interleaved acceleration R=3, TE=1.04ms, TR=2.5ms, TD=40ms, flip angle 50^o, FISP readout. Gadolinium [Gd] contrast agent (XX and XH: gadoterate meglumine, Dotarem; Guerbet, Paris, France; LTHT: Gadovist, Leverkusen, Germany) was administered as a bolus of 0.05 mmol/kg at 4 ml/sec with 20 ml saline flush using power injectors (Medrad MRXperion Injection System, Bayer). For stress perfusion, adenosine was administered by continuous intravenous infusion for 4 min at a dose of 140 μg/kg/min before contrast injection (increased to 175 μg/kg/min for a further 2 minutes based on patient's response). The imaging started by acquiring three proton density weighted images, followed by saturation recovery images. Every perfusion image was acquired as a 2D image cutting through the heart and this acquisition was repeated for every heart beat to capture the contrast passage, typically lasting 60 heart beats. This resulted in the 2D+T time series where images were acquired consecutively in time. Details of imaging and perfusion mapping can be found in Kellman et al (3). Datasets were acquired using both 1.5 T (four MAGNETOM Aera, Siemens AG Healthcare, Erlangen, Germany) and 3 T (three MAGNETOM Prisma, Siemens AG Healthcare) MR scanners.

Appendix E2: Data preparation and labeling

Perfusion image series underwent motion and surface coil inhomogeneity correction. Motion correction utilized non-rigid image registration in an iterative manner. To compensate for substantial image contrast variation during the contrast bolus passage, instead of directly

820 Jorie Blvd., Suite 200, Oak Brook, IL, 60523, 630-481-1071, rad-ai@rsna.org

registering perfusion images against each other, synthetic perfusion series were derived from a Karhunen-Loève transform. Motion correction was achieved by registering perfusion images pairwise with the synthetic series. The detailed algorithm was presented in Xue et al (4). After correcting respiratory motion, surface coil inhomogeneity was corrected using the proton density images and the normalized intensities were converted to gadolinium concentration units (mmol/L) (3). To compensate for heart rate variation and mis-triggering, the perfusion series was temporally resampled using linear interpolation which also compensated for possible missed triggers. This interpolation resulted in a fixed sampling corresponding to a heart rate of 120 bpm. The temporal resampling step did not lead to spatial blurring since it was performed after motion correction.

Since the gadolinium concentration series was corrected for signal nonlinearity and surface coil inhomogeneity, it had the benefit of reducing the dynamic range and providing a fixed signal range for neural nets, compared to perfusion intensity images. This image series was spatially upsampled to 1.0 mm^2 spatial resolution and the central field of view (176 × 176 mm^2) was cropped. The left ventricular (LV) blood pool was detected from the arterial input function series which was imaged at the basal plane at diastole. The location of the LV blood pool from this step was used to center the cropped image (9). For the short axis perfusion slices, the LV endo- and epicardial boundaries were manually traced, together with the right ventricle (RV) (Fig. 1). The RV insertion point was determined from the segmented right ventricular and LV center as the rightmost pixel. The training and test datasets were carefully labeled by one operator (XX, 10 years of experience in perfusion imaging).

820 Jorie Blvd., Suite 200, Oak Brook, IL, 60523, 630-481-1071, rad-ai@rsna.org

Appendix E3: Model, Training and Inline Integration

Details of Neural Net Model

The first 48 images were empirically selected, starting at the first saturation recovery image. This resulted in an image array of 176 × 176 × 48 per section, covering the first-pass bolus passage of injected contrast agent. A total of 262800 2D images were then used for training the neural networks**.** The U-net semantic segmentation architecture (11,12) was adopted for the perfusion segmentation. The neural net (Fig. 2) consisted of downsampling and upsampling layers, each including a number of ResNet blocks (13). The downsampling and upsampling operations were inserted between layers to change the spatial resolution. For simplicity, two convolutional layer operations with the same number of output filters were added to each block, together with Batch Normalization (14) and LeakyRelu (15) nonlinearity. All convolutional layers used a 3 × 3 kernel with stride of 1 and padding of 1. Following the principle of U-net, the downsampling and upsampling layers were connected with Skip-connections. The spatial resolution was reduced by going through the down-sampling branch with the number of convolution filters increased. The up-sampling branch increased the spatial resolution and reduced the number of filters. The network was able to learn features from this coarse-to-fine pyramid thereby selecting an optimal filter combination to minimize the loss function.

The final convolutional layer output was a 176 × 176 × 3 array of scores representing segmented classes, which were converted to probability through a softmax operation. Establishing the anatomical context of LV cavity, myocardium, and right ventricle was facilitated by using a single trained CNN. The loss function was a weighted sum of cross-entropy and the intersection over union. This cost function optimizes the overlap between the detected mask and ground-truth while maximizing the probability for a pixel to be correctly

820 Jorie Blvd., Suite 200, Oak Brook, IL, 60523, 630-481-1071, rad-ai@rsna.org

classified, previously shown to improve segmentation accuracy (26). The trained CNN models were applied to both stress and rest test scans.

Training and Hyperparameter Search

The data for training was split into a training set (87.5% of all studies) and a validation set (12.5% of all studies) and the CNN model and optimization was implemented using PyTorch (16). Training was performed on a Linux PC (Ubuntu 18.04) with four NVIDIA GTX 2080Ti GPU cards. ADAM optimization was used with initial learning rate equal to 0.001 (beta = 0.9 and 0.999; epsilon = $1 \cdot 10^{-8}$). Learning rate was reduced by a factor of 2 for every 10 epochs. Training took 60 epochs and best model was selected as the one giving best performance on the validation set.

A hyperparameter search was conducted to test different network parameter combinations (2 to 4 resolution layers, 2 to 4 blocks per layer, and number of convolution filters of either 64, 128 and 256). After the hyperparameter search, best performance was found for an architecture containing two down-sampling and up-sampling layers, with two ResNet blocks for the first layer and three blocks for the second. This led to a deep net with 23 convolution layers in total. On the tested hardware, training took approximately 8 hours for 60 epochs.

Inline integration of trained models

The trained model was integrated to run on MR scanners using the Gadgetron Inline AI (7) streaming software which provides flexible interfaces to load pre-trained neural networks and apply them on incoming new data. This involved transferring model objects from Pytorch to C++ and passed data from C++ to Pytorch modules. Model inference was chosen to utilize a central processing unit (CPU) which was sufficiently fast for clinical usage.

820 Jorie Blvd., Suite 200, Oak Brook, IL, 60523, 630-481-1071, rad-ai@rsna.org

Perfusion segmentation functionality was performed after inline perfusion mapping. As soon as a perfusion scan was configured, the pre-trained model was loaded into the Gadgetron runtime environment. Following image reconstruction and pre-processing, models were applied to the incoming 2D+T image series for each slice. Resulting segmentation was used to generate the 16-sector measurement of perfusion and produce a summary report. All steps were fully automatic without any user interaction. A screenshot (Fig. 3) illustrates the perfusion mapping with overlaid CNN based segmentation and AHA report, applied to a patient with reduced regional perfusion. This is a "one-click" solution for automated analysis of quantitative perfusion flow mapping. Trained models were tested on two computing servers for timing. Xeon Gold: 2×Intel Xeon Gold 6152 CPU @ 2.1GHz, released in 2017, 192 GB RAM. Xeon E5: Intel Xeon E5-2680 CPU, released in 2012 and 64G RAM.

820 Jorie Blvd., Suite 200, Oak Brook, IL, 60523, 630-481-1071, rad-ai@rsna.org

Availability of data and material

The raw data that support the findings of this study are available from the corresponding author upon reasonable request subject to restriction on use by the Office of Human Subjects Research. The source file to train the CNN model and example datasets are shared at https://github.com/xueh2/QPerf.git.

820 Jorie Blvd., Suite 200, Oak Brook, IL, 60523, 630-481-1071, rad-ai@rsna.org

Funding

Authors' contributions

820 Jorie Blvd., Suite 200, Oak Brook, IL, 60523, 630-481-1071, rad-ai@rsna.org

References

1. Nagel E, Greenwood JP, McCann GP, et al. Magnetic resonance perfusion or fractional flow reserve in coronary disease. N Engl J Med. 2019;380(25):2418–2428.

2. Kotecha T, Martinez-Naharro A, Boldrini M, et al. Automated Pixel-Wise Quantitative Myocardial Perfusion Mapping by CMR to Detect Obstructive Coronary Artery Disease and Coronary Microvascular Dysfunction. JACC Cardiovasc Imaging. 2019;12(10):1958–1969.

3. Kellman P, Hansen MS, Nielles-Vallespin S, et al. Myocardial perfusion cardiovascular magnetic resonance: optimized dual sequence and reconstruction for quantification. J Cardiovasc Magn Reson. 2017;19(1):43.

4. Xue H, Brown LAE, Nielles-Vallespin S, Plein S, Kellman P. Automatic in-line quantitative myocardial perfusion mapping: Processing algorithm and implementation. Magn Reson Med. 2020;83(2):712–730.

5. Zorach B, Shaw PW, Bourque J, et al. Quantitative cardiovascular magnetic resonance perfusion imaging identifies reduced flow reserve in microvascular coronary artery disease. J Cardiovasc Magn Reson. Journal of Cardiovascular Magnetic Resonance; 2018;20(1):1–8.

6. Acampa W, Petretta M, Evangelista L, et al. Myocardial perfusion imaging and risk classification for coronary heart disease in diabetic patients. The IDIS study: A prospective, multicentre trial. Eur J Nucl Med Mol Imaging. 2012;39(3):387–395.

7. Xue H, Davies R, Hansen D, et al. Gadgetron Inline AI : Effective Model inference on MR scanner. ISMRM. 2019. p. 4837.

8. Knott KD, Seraphim A, Augusto JB, et al. The Prognostic Significance of Quantitative Myocardial Perfusion: An Artificial Intelligence-Based Approach Using Perfusion Mapping. Circulation. 2020;1282–1291.

9. Xue H, Tseng E, Knott KD, et al. Automated detection of left ventricle in arterial input function images for inline perfusion mapping using deep learning: A study of 15,000 patients. Magn Reson Med. 2020;(March):1–13.

10. Bluemke DA, Moy L, Bredella MA, et al. Assessing radiology research on artificial intelligence: A brief guide for authors, reviewers, and readers-from the Radiology Editorial Board. Radiology. 2020;294(2):487–489.

11. Ronneberger O, Fischer P, Brox T. U-net: Convolutional networks for biomedical

820 Jorie Blvd., Suite 200, Oak Brook, IL, 60523, 630-481-1071, rad-ai@rsna.org

image segmentation. Lect Notes Comput Sci. 2015;9351:234–241.

12. Zhang Z, Liu Q, Wang Y. Road Extraction by Deep Residual U-Net. IEEE Geosci Remote Sens Lett. 2018;1–5.

13. Xie S, Girshick R, Dollár P, Tu Z, He K. Aggregated residual transformations for deep neural networks. CVPR. 2017;5987–5995.

14. Ioffe S, Szegedy C. Batch Normalization: Accelerating Deep Network Training by Reducing Internal Covariate Shift. ICML. 2016;10(6):730–743.

15. Maas AL, Hannun AY, Ng AY. Rectifier nonlinearities improve neural network acoustic models. ICML. 2013;28.

16. Paszke A, Gross S, Chintala S, et al. Automatic differentiation in pytorch. 31st Conf Neural Inf Process Syst. 2017. p. 1–8.

17. Xue H, Shah S, Greiser A, et al. Motion correction for myocardial T1 mapping using image registration with synthetic image estimation. Magn Reson Med. 2012;67:1644–1655.

18. Huttenlocher DP, Rucklidge WJ, Klanderman GA. Comparing images using the Hausdorff distance under translation. Proc. IEEE Comput. Soc. Conf. Comput. Vis. Pattern Recognit. 1992. p. 654–656.

19. Scannell CM, Veta M, Villa ADM, et al. Deep-Learning-Based Preprocessing for Quantitative Myocardial Perfusion MRI. J Magn Reson Imaging. 2020;51(6):1689–1696.

20. Lin TY, Goyal P, Girshick R, He K, Dollar P. Focal Loss for Dense Object Detection. IEEE Trans Pattern Anal Mach Intell. 2020;42(2):318–327.

21. Peng P, Lekadir K, Gooya A, Shao L, Petersen SE, Frangi AF. A review of heart chamber segmentation for structural and functional analysis using cardiac magnetic resonance imaging. Magn Reson Mater Physics, Biol Med. Springer Berlin Heidelberg; 2016;29(2):155–195.

22. Bernard O, Lalande A, Zotti C, et al. Deep Learning Techniques for Automatic MRI Cardiac Multi-Structures Segmentation and Diagnosis: Is the Problem Solved? IEEE Trans Med Imaging. 2018;37(11):2514–2525.

23. Bai W, Sinclair M, Tarroni G, et al. Automated cardiovascular magnetic resonance

820 Jorie Blvd., Suite 200, Oak Brook, IL, 60523, 630-481-1071, rad-ai@rsna.org

image analysis with fully convolutional networks. J Cardiovasc Magn Reson. Journal of Cardiovascular Magnetic Resonance; 2018;20(65).

24. Moccia S, Banali R, Martini C, et al. Development and testing of a deep learning-based strategy for scar segmentation on CMR-LGE images. Magn Reson Mater Physics, Biol Med. Springer International Publishing; 2019;32(2):187–195.

25. Camaioni C, Knott KD, Augusto JB, et al. Inline perfusion mapping provides insights into the disease mechanism in hypertrophic cardiomyopathy. Heart. 2019;824–829.

26. Milletari F, Navab N, Ahmadi SA. V-Net: Fully convolutional neural networks for volumetric medical image segmentation. 4th Int Conf 3D Vis. 2016. p. 565–571.

820 Jorie Blvd., Suite 200, Oak Brook, IL, 60523, 630-481-1071, rad-ai@rsna.org

Table 1. Dataset Information

	Sites	#Patients	#Stress scan	#Rest scan
Training	XX	475	432	475
	XH	345	219	345
	XTH	214	140	214
Total		***1034***	***791***	***1034***
Test	XX	54	46	54
	XH	13	11	13
	XTH	38	38	38
Total		***105***	***95***	***105***

820 Jorie Blvd., Suite 200, Oak Brook, IL, 60523, 630-481-1071, rad-ai@rsna.org

List of Captions

Figure 1 Data preparation for performing convolutional neural network-based segmentation used in this study. Respiratory motion correction of perfusion images provides pixel-wise alignment of myocardial tissue. Image intensities are corrected for surface coil inhomogeneity and converted to gadolinium concentration units. Images are resampled to a fixed temporal and spatial resolution and cropped around the left ventricular cavity. The resulting 2D+T time series of images is input for convolutional neural network training, together with supplied manual labeling.

Figure 2 Schematic plot of the convolutional neural network trained in this study. This network consists of downsampling and upsampling layers. Each layer includes a number of ResNet blocks. More layers and blocks can be inserted into the convolutional neural network to increase its depth. In the example illustration, two layers are used with two blocks for each layer. The total number of convolution blocks is 23. BN = Batch Normalization, C = concatenate filter response, CNN = convolutional neural network, CONV = convolution, LV =left ventricle, RELU = rectified linear units, RV = right ventricle

Figure 3 Example screenshot for a patient undergoing an adenosine stress study, demonstrating the proposed inline analysis solution on a MR scanner. Stress maps show regional flow reduction in septal and inferior sectors. The determined right ventricular insertion was used to split myocardium to American Heart Association (AHA) sectors, with the contours overlaid to mark territories. The inline reporting further produced a 16-sector AHA bulls-eye plot with global and per-sector flow measures reported in a table.

Figure 4 Example adenosine stress perfusion images and myocardial blood flow (MBF) maps illustrating segmentation in the format of derived American Heart Association sector contours overlaid on flow maps. For each case, the first row are the images in gadolinium units and the second row are the MBF maps. Sector contours were overlaid to mark three territories for left anterior coronary artery (yellow), right coronary artery (green), and left circumflex (red). **(a)** Patient with single vessel obstructive coronary artery disease in right coronary artery territory. Papillary muscle was not included in segmentation, **(b)**

820 Jorie Blvd., Suite 200, Oak Brook, IL, 60523, 630-481-1071, rad-ai@rsna.org

patient with hypertrophic cardiomyopathy illustrating that the convolutional neural network-based segmentation works with thick myocardium and small cavity. The epicardial fat was correctly excluded.

Figure 5 Bland-Altman plots for independent test dataset **(a)** global mean myocardial blood flow (MBF) and **(b)** per-sector measures. No significant differences were found between convolutional neural network derived results and manual measures. The dotted lines mark the 95% confidence range. CNN = convolutional neural network.

820 Jorie Blvd., Suite 200, Oak Brook, IL, 60523, 630-481-1071, rad-ai@rsna.org

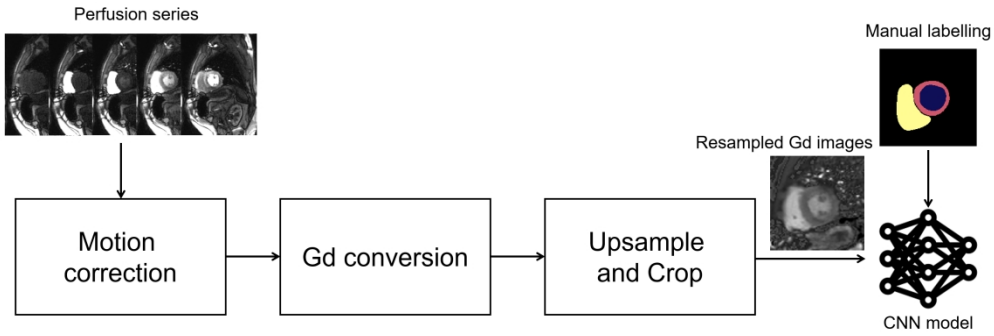

Figure 1 Data preparation for performing convolutional neural network-based segmentation used in this study. Respiratory motion correction of perfusion images provides pixel-wise alignment of myocardial tissue. Image intensities are corrected for surface coil inhomogeneity and converted to gadolinium concentration units. Images are resampled to a fixed temporal and spatial resolution and cropped around the left ventricular cavity. The resulting 2D+T time series of images is input for convolutional neural network training, together with supplied manual labeling.

262x88mm (300 x 300 DPI)

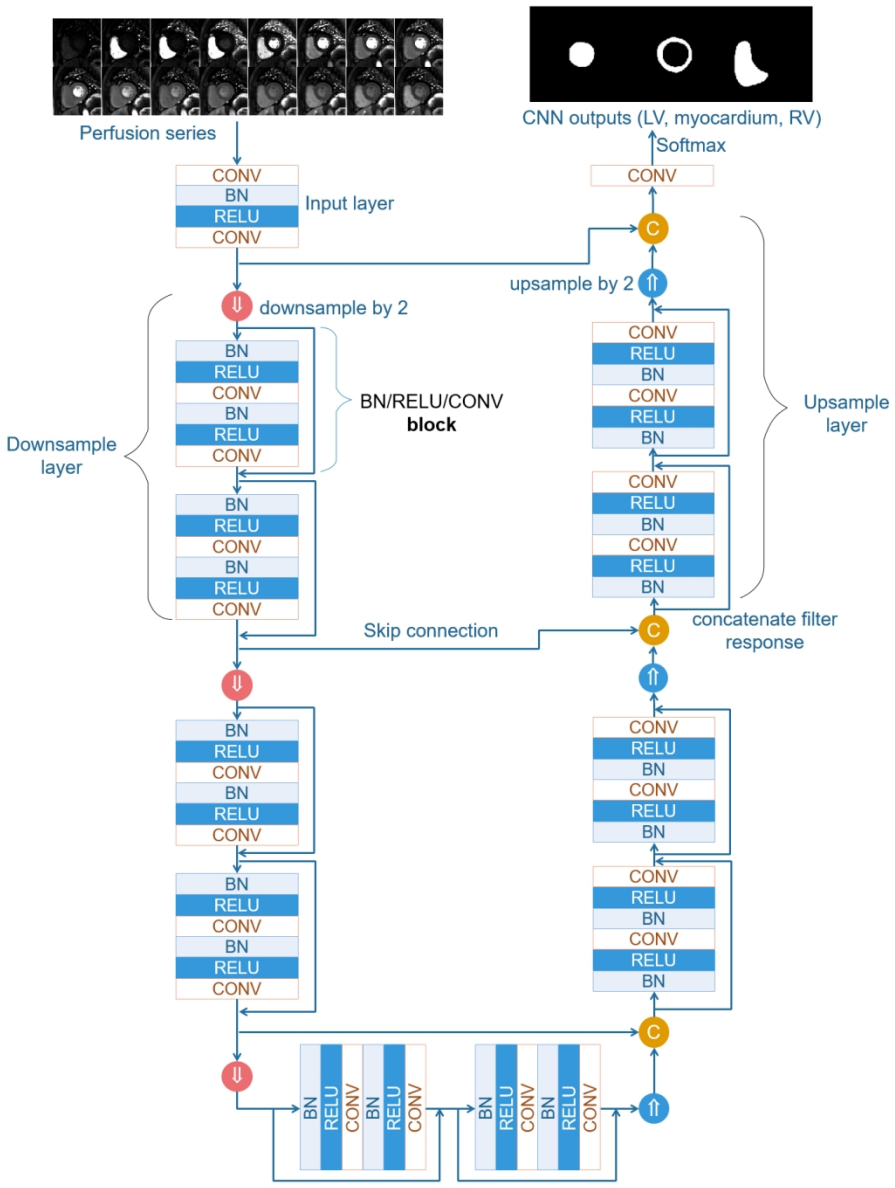

Figure 2 Schematic plot of the convolutional neural network trained in this study. This network consists of downsampling and upsampling layers. Each layer includes a number of ResNet blocks. More layers and blocks can be inserted into the convolutional neural network to increase its depth. In the example illustration, two layers are used with two blocks for each layer. The total number of convolution blocks is 23. BN = Batch Normalization, C = concatenate filter response, CNN = convolutional neural network, CONV = convolution, LV =left ventricle, RELU = rectified linear units, RV = right ventricle.

119x159mm (300 x 300 DPI)

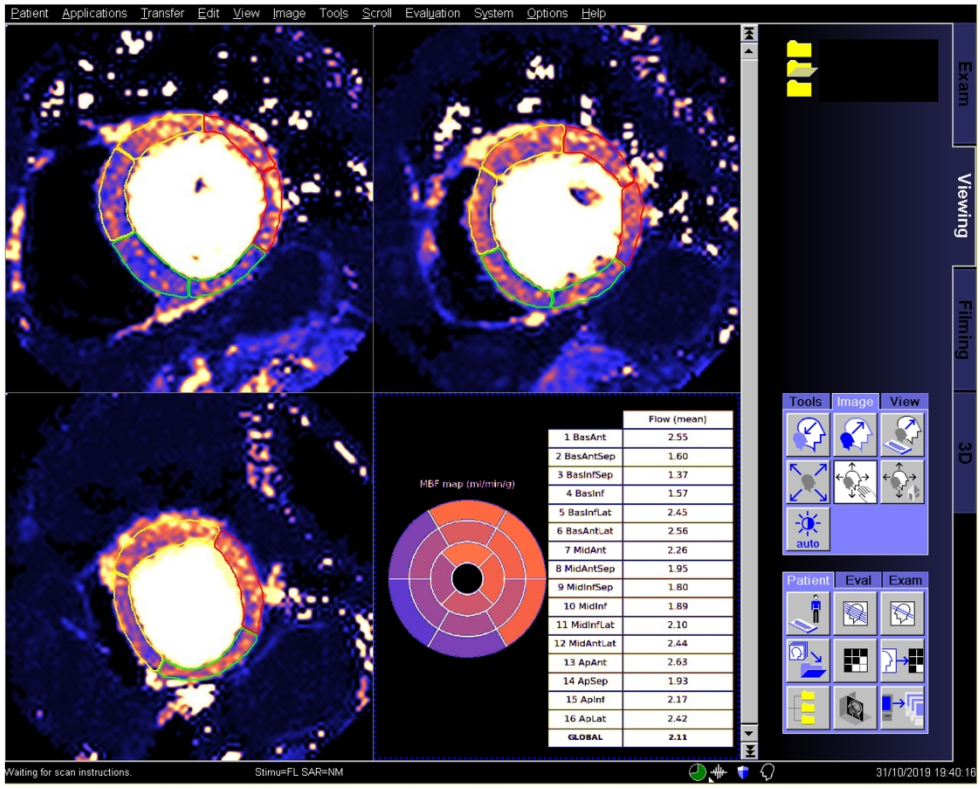

Figure 3 Example screenshot for a patient undergoing an adenosine stress study, demonstrating the proposed inline analysis solution on a MR scanner. Stress maps show regional flow reduction in septal and inferior sectors. The determined right ventricular insertion was used to split myocardium to American Heart Association (AHA) sectors, with the contours overlaid to mark territories. The inline reporting further produced a 16-sector AHA bulls-eye plot with global and per-sector flow measures reported in a table.

261x208mm (300 x 300 DPI)

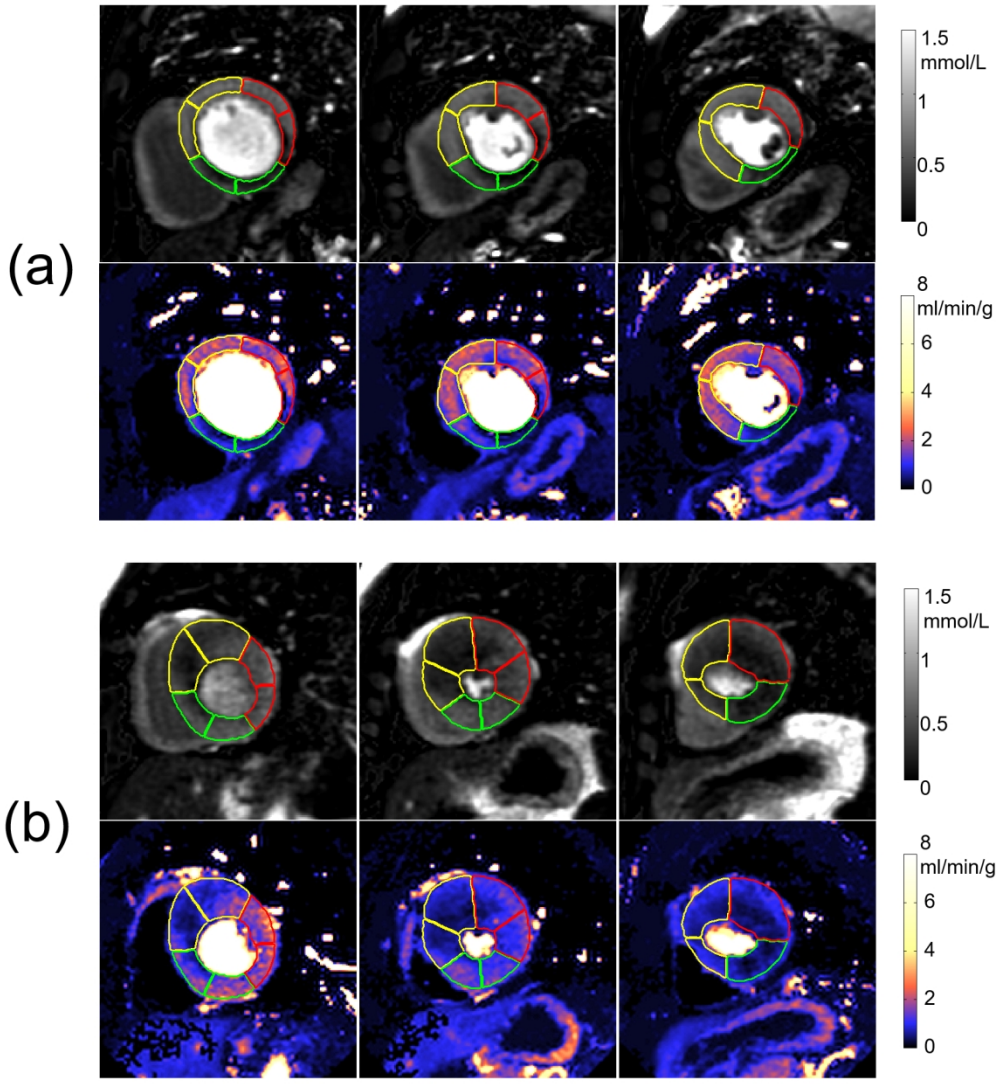

Figure 4 Example adenosine stress perfusion images and myocardial blood flow (MBF) maps illustrating segmentation in the format of derived American Heart Association sector contours overlaid on flow maps. For each case, the first row are the images in gadolinium units and the second row are the MBF maps. Sector contours were overlaid to mark three territories for left anterior coronary artery (yellow), right coronary artery (green), and left circumflex (red). (a) Patient with single vessel obstructive coronary artery disease in right coronary artery territory. Papillary muscle was not included in segmentation, (b) patient with hypertrophic cardiomyopathy illustrating that the convolutional neural network-based segmentation works with thick myocardium and small cavity. The epicardial fat was correctly excluded.

150x163mm (300 x 300 DPI)

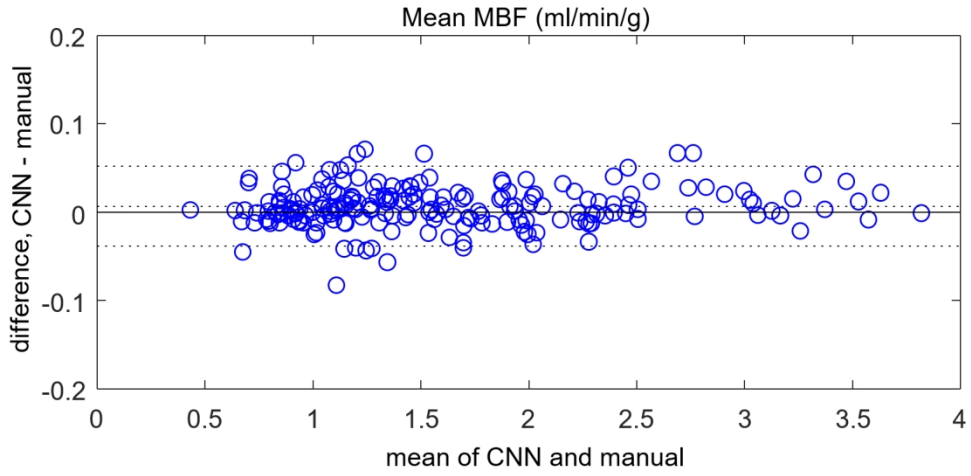

(a) Bland-Altman plot of global MBF

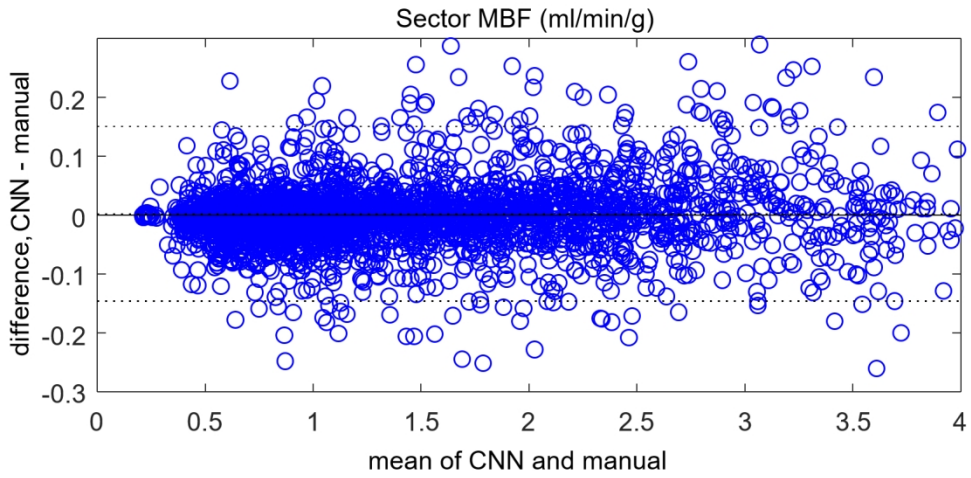

(b) Bland-Altman plot of per-sector MBF

Figure 5 Bland-Altman plots for independent test dataset (a) global mean myocardial blood flow (MBF) and (b) per-sector measures. No significant differences were found between convolutional neural network derived results and manual measures. The dotted lines mark the 95% confidence range. CNN = convolutional neural network.

145x159mm (300 x 300 DPI)